Pergamon

Geochimica et Cosmochimica Acta, Vol. 68, No. 1, pp. 101–113, 2004

0016-7037/04 $30.00 + .00

doi:10.1016/S0016-7037(03)00258-8

Formation of monazite via prograde metamorphic reactions among common silicates: Implications for age determinations

MATTHEW J. KOHN* and MARGARET A. MALLOY†
Department of Geological Sciences, University of South Carolina, Columbia, SC 29208, USA

(*Received June* 6, 2002; revised 1 April 2003; *accepted in revised form April* 1, 2003)

Abstract—Three lines of evidence from schists of the Great Smoky Mountains, NC, indicate that isogradic monazite growth occurred at the staurolite-in isograd at ~600°C: (1) Monazite is virtually absent below the staurolite-in isograd, but is ubiquitous (several hundred grains per thin section) in staurolite- and kyanite-grade rocks. (2) Many monazite grains are spatially associated with biotite coronas around garnets, formed via the reaction Garnet + Chlorite + Muscovite = Biotite + Plagioclase + Staurolite + H_2O. (3) Garnets contain high-Y annuli that result from prograde dissolution of garnet via the staurolite-in reaction, followed by regrowth, and rare monazite inclusions occur immediately outside the annulus and in the matrix, but not in the garnet core. Larger monazite grains also exhibit quasi-continuous Th zoning with high Th cores and low Th rims, consistent with monazite growth via a single reaction and fractional crystallization during prograde growth. Common silicates may host sufficient P and LREEs that reactions among them can produce observable LREE phosphate. Specifically phosphorus contents of garnet and plagioclase are hundreds of parts per million, and dissolution of garnet and recrystallization of plagioclase could form thousands of phosphate grains several micrometers in diameter per thin section. LREEs may be more limiting, but sheet silicates and plagioclase can contain tens to ~100 (?) ppm LREE, so recrystallization of these silicates to lower LREE contents could produce hundreds of grains of monazite per thin section. Monazite ages, determined via electron and ion microprobes, are ~400 Ma, directly linking prograde Barrovian metamorphism of the Western Blue Ridge with the "Acadian" orogeny, in contrast to previous interpretations that metamorphism was "Taconian" (~450 Ma). Interpretation of ages from metamorphic monazite grains will require prior chemical characterization and identification of relevant monazite-forming reactions, including reactions previously viewed as involving solely common silicates. *Copyright © 2004 Elsevier Ltd*

1. INTRODUCTION

Monazite ([LREE, Th]PO_4) is a common accessory mineral in metapelitic schists, and has long been used for metamorphic geochronology. Its high concentrations of U (up to 1 wt.%) and Th (up to 20 wt.%), low initial Pb contents (e.g., Parrish, 1990) yet high retentivity for radiogenic Pb (Smith and Giletti, 1997; Cherniak et al., 2000) make it ideal for U-Th-Pb age determinations via TIMS or ion microprobe. Older grains can be dated based on bulk chemical measurements of U, Th, and Pb by using the electron probe (e.g., Montel et al., 1996). Its chemical and diffusional advantages notwithstanding, a serious problem with monazite age determinations is interpreting what a particular age represents. Some monazite grains have withstood melting (Copeland et al., 1988; Harrison et al., 1995; Watt, 1995), again attesting to high resistance to Pb-loss via diffusion, whereas other grains betray a profound susceptibility to dissolution and reprecipitation in low-*T* hydrothermal environments (Townsend et al., 2000; Rasmussen et al., 2001). Further complications arise for regional metamorphic rocks in identifying the *P-T* conditions at which monazite forms. New monazite growth has been documented at greenschist- (≤450°C; Franz et al., 1996; Townsend et al., 2000; Catlos et al., 2001), midamphibolite- (~525–575°C; Smith and Barreiro, 1990; Kingsbury et al., 1993; Ferry, 2000; Pyle and Spear, 2003; Wing et al., 2003), and uppermost amphibolite- to granulite-facies conditions (>700°C; Bingen et al., 1996; Bea and Montero, 1999; Pyle et al., 2001; Pyle and Spear, 2003), with differences in the *P-T* of appearance presumably reflecting differing bulk compositions and mineralogies. Indeed, many workers ascribe monazite growth to the prograde breakdown of allanite (LREE-silicate; Smith and Barreiro, 1990; Kingsbury et al., 1993; Bingen et al., 1996; Ferry, 2000; Catlos et al., 2001; Wing et al., 2003), assuming P is derived from apatite. Thus, the temperature of monazite-in can range from ~450°C (immediately below the garnet-in isograd) to ~575°C or higher (the staurolite- and/or aluminosilicate-in isograds), and monazite could potentially dissolve and reprecipitate over an even larger range of temperatures during prograde and retrograde processes.

The importance of silicate reactions in forming monazite is commonly evaluated based on spatial distributions of monazite over a range of grades (e.g., Smith and Barreiro, 1990; Franz et al., 1996; Ferry, 2000; Wing et al., 2003). Whereas spatial distributions of monazite are certainly useful in our study area, a more important result of our work is that mineral textures and intracrystalline chemical zoning patterns pinpoint major production of monazite at the prograde, staurolite-in silicate reaction. That is, the monazite-forming reaction does not have to be assumed from regional distributions, but rather can be inferred from textures and chemical zoning in a specific rock. This approach was used by Pyle and Spear (2003) in uppermost amphibolite-facies rocks from an outcrop in New Hampshire,

---

* Author to whom correspondence should be addressed (mjk@geol.sc.edu).

† *Present address:* Department of Earth and Environmental Sciences, Lehigh University, Bethlehem, PA 18015, USA.

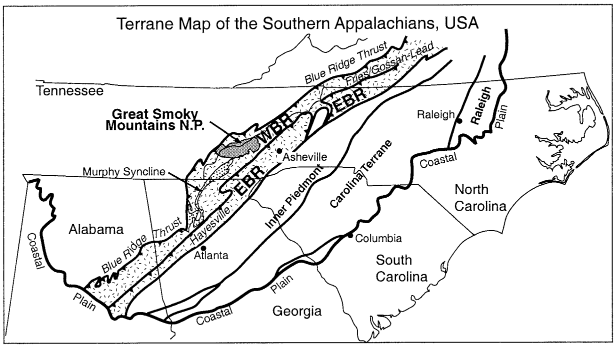

Fig. 1. Generalized terrane map of the southern Appalachians, showing position of the Great Smoky Mountains National Park within the Western Blue Ridge. After Hatcher (1987).

USA. However, their study implicated melting reactions, which has a major influence on phosphorus partitioning, and key participation of apatite. In contrast, our rocks are not anatectic, and our observations further suggest that participation of other accessory minerals was not necessary to form monazite. That is, isogradic reactions among major silicates alone may have profound effects on the appearance and distribution of monazite. This implies that age interpretation will require detailed chemical and textural characterization of not only monazite, but also other common silicates in the rock.

2. GEOLOGIC BACKGROUND

The Great Smoky Mountains occupy the Western Blue Ridge (WBR) geologic province, which is the westernmost metamorphic belt in a ~250-km wide series of metamorphic and plutonic belts stretching from the mountains of Tennessee and North Carolina to the coastal plain (Fig. 1). The geology and distribution of metamorphic index minerals are shown in Figure 2. At the latitude of the Smokies, the WBR is separated from the Valley and Ridge to the west by the brittle Alleghanian Great Smoky Fault (part of the Blue Ridge Thrust system), and from the Eastern Blue Ridge (EBR) to the east by the Hayesville Fault, which appears to predate the main Barrovian metamorphism (e.g., Hatcher, 1987). Tectonostratigraphically, metamorphic rocks of the Smokies consist of a Grenvillian basement complex, overlain by metasedimentary rocks of the Ocoee Series (Snowbird, Great Smoky, and Walden Creek Groups). The Thunderhead Sandstone and Anakeesta Formation (Great Smoky Group) dominate outcrops in the national park and were the focus of this study. The Thunderhead Sandstone is mainly a metarkose, interbedded at a decimeter to meter scale with cm- to dm-thick aluminous schist. Towards

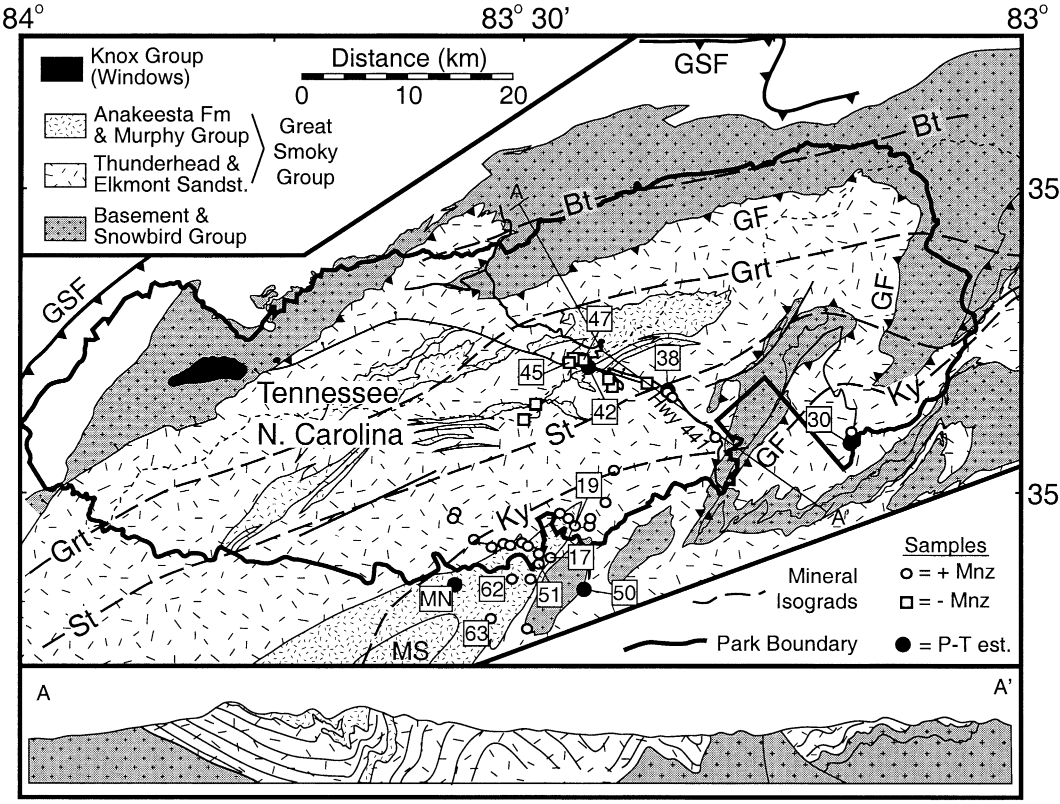

Fig. 2. Geologic and geographic map of Great Smoky Mountains area showing major faults and distribution of lithologies and metamorphic grades. Metamorphism increases towards the south and is best evidenced within the Thunderhead Sandstone and Anakeesta Formation. Abbreviations: GSF = Great Smoky Fault (Alleghanian thrust), GF = Greenbrier Fault (Premetamorphic thrust), MS = Murphy Syncline. Black dots are locations of *P-T* calculations (this study; Mohr and Newton, 1983). Cross-section shows refolding of pervasive, early fabric by upright folds.

the top of the Thunderhead Sandstone, schists become increasingly graphitic, and the unit grades into the Anakeesta Formation, a graphitic and sulfidic schist with interbedded quartzite.

Metamorphic isograds are well defined by the pelitic schists of the Thunderhead Sandstone and Anakeesta Formation (Hadley and Goldsmith, 1963). The biotite, garnet, staurolite, and kyanite isograds are subparallel to the NE-SW–trending structural grain, and metamorphic grade increases progressively to the southeast, ultimately culminating in lower-granulite facies (sillimanite–K-feldspar) rocks of the EBR. In general, lower-grade outcrops in the park are more graphitic, perhaps signaling a general trend in bulk compositions with increasing metamorphic grade. Metamorphic *P-T* conditions have been previously calculated for only one kyanite-grade rock in the area, and are ~580°C and 6.6 kbar (Mohr and Newton, 1983).

Prograde and/or peak metamorphic ages have not been published for the Smokies, and are controversial. Traditionally metamorphism has been viewed as Taconian in age (~450 Ma) mainly because (1) whole-rock and hornblende $^{40}Ar/^{39}Ar$ spectra in the region were interpreted as indicative of recrystallization at 440 to 460 Ma and cooling through the hornblende blocking temperature (~500°C; Harrison, 1981) at ~425 Ma (Dallmeyer, 1975, 1988; Connelly and Dallmeyer, 1993), (2) a thick clastic wedge (the Blountian wedge) developed in Eastern Tennessee in the mid-Ordovician and was interpreted as the sedimentary response to southern Appalachian Taconian orogenesis and loading (Rodgers, 1953, 1971; Neuman, 1955), and (3) the Taconic Orogeny is the first post-Grenvillian orogenic event that affected the Laurentian margin, and so one would expect the westernmost (i.e., most internal) metamorphic belt to be oldest. However, (1) studies of hornblende from overprinted basement rocks commonly identify excess ^{40}Ar contamination, yielding reinterpreted younger ages (e.g., Hames et al., 1991; Cumbest et al, 1994), (2) Blue Ridge metamorphic rocks were transported westward by several hundred km during later Alleghanian thrusting (Cook et al., 1979, 1981), complicating direct linkage between western Blue Ridge metamorphism and Blountian sedimentation, (3) rocks that overlie the Great Smoky Group and that share deformation fabrics with it (Woodward et al., 1991; Connelly and Woodward, 1992) yield sparse Siluro-Devonian microfossils (i.e., post-Taconian; Unrug and Unrug, 1990; Unrug et al., 1991, 2000), and (4) rocks from the Murphy syncline (SW of the park) are stratigraphically, structurally, and metamorphically continuous with Great Smoky rocks, and have yielded a preliminary U-Pb (TIMS) staurolite age of 412 ± 6 Ma (Brosky and Odom, 2002). By comparison to the northern Appalachians events to the north (e.g., in New England), the younger ages have been ascribed to the ~400-Ma "Acadian" orogeny, although the origin of a southern Acadian event is unclear (Hibbard, 2000).

3. METHODS

Major and trace element concentrations were measured by using the fully automated Cameca SX50 electron microprobe, housed at University of South Carolina's Electron Microscopy Center. Qualitative X-ray maps were collected first on garnet and monazite grains to delineate geochemically significant zones, and to guide quantitative spot analyses. Natural silicates and oxides were used as standards for major elements. Synthetic YAG, CeO_2, La-doped glass (Drake and Weill, 1972), U metal, ThO_2, and $PbSiO_3$ were used for standardizing Y, Ce, La, U, Th, and Pb respectively. A natural Pb-phosphate was also checked as a Pb standard, and results are indistinguishable from those obtained using $PbSiO_3$. For monazites, we were interested primarily in U-Th-Pb dating, rather than precisely defining REE concentrations. Consequently, of the REE's, we only analyzed Ce and La, and defined the rest as "Nd" by difference from 100%. ZAF corrections are imperceptibly affected by ignoring the heavier REE's, which speeds analysis by a few minutes per spot. Count times, currents, X-ray lines, and trace element counting statistics errors are summarized in Table 1. Spot sizes were 1 μm for major element analyses of silicates except plagioclase and muscovite (5-μm diameter), and 5 to 10 μm for monazite analyses.

Table 1. Operating conditions for electron microprobe analyses.

Element	Silicate-major[a]	Monazite[a]
Si (Kα)	20 nA/20 s/TAP	40 nA/40 s/TAP
Ti (Kα)	20 nA/20 s/PET	
Al (Kα)	20 nA/20 s/TAP	
Mg (Kα)	20 nA/20 s/TAP	
Fe (Kα)	20 nA/20 s/LIF	
Mn (Kα)	20 nA/20 s/LIF	
Ca (Kα)	20 nA/20 s/PET	40 nA/20 s/PET
Na (Kα)	20 nA/20 s/TAP	
K (Kα)	20 nA/20 s/PET	
Y (Lα)		40 nA/40 s/PET
Ce (Lα)		40 nA/20 s/LIF
La (Lα)		40 nA/20 s/LIF
P (Kα)		40 nA/20 s/PET
U (Mβ)		200 nA/120 s/PET
Th (Mα)		200 nA/120 s/PET
Pb (Mα)		200 nA/240 s/PET

[a] Values refer to Faraday current, count time, and crystal used. For Pb, this corresponds to a counting statistics uncertainty of ±65 ppm ($\pm 1\sigma$).

Initial attempts at measuring monazite ages met with analytical problems. Some well-polished grains gave ages that were indistinguishable within counting statistics uncertainties, whereas poorly polished samples sometimes yielded age scatter that was 2 to 3 times greater, although with the same mean age. We subsequently found that a focused beam caused current drift in some samples during analysis, apparently because of contamination of the C-coat, whereas others showed no drift whatsoever, and could be reliably analyzed in the same spot multiple times. Consequently, we now restrict analysis to well-polished grains, and monitor beam current during every analysis to verify that current drift is not a problem. We originally reported an absence of any resolvable age variation among monazite grains in different samples or in different habits (Kohn, 2001), suggesting that all monazites have similar ages, at least within the precision of the electron microprobe. Whereas that conclusion is likely robust (i.e., a single set of analytical conditions consistently yields statistically indistinguishable ages among samples analyzed on a single day), the accuracy of many of those reported ages needs reevaluation in light of recent revisions to analytical protocols (Pyle et al., 2002; see also Appendix). Consequently, we restrict consideration to a few, well-polished samples analyzed recently that showed no current drift during analysis, and for which strict standardization and analytical protocols were followed that minimize potential inaccuracies.

Electron microprobe ages for monazites were calculated from bulk U-Th-Pb contents assuming that ^{235}U and ^{238}U were in normal relative abundance (1/137.88), that all Pb was radiogenic (mostly ^{206}Pb from Th decay, but also ^{207}Pb and ^{208}Pb from U decay), and that the U-Pb and Th-Pb systems were concordant (Montel et al., 1996; Suzuki and Adachi, 1998; Williams et al., 1999; Scherrer et al., 2000). The accuracy of this approach is supported by two general observations (Montel et al., 1996): (1) Most monazites have extremely low initial Pb, typically < 1 ppm total as determined by TIMS (e.g., Heaman and Parrish, 1990; Parrish, 1990). Typical Pb contents in Paleozoic monazites are many hundreds to thousands of parts per million, and subtracting 1 ppm total common Pb in age calculations affects estimated ages by < 1 Ma. Because the ±65-ppm counting statistics error in Pb corresponds to an age uncertainty of ~±15 to 30 Ma ($\pm 1\sigma$), a common

Pb correction for this approach is ordinarily unneeded. (2) Many monazites are in fact concordant. The main problems with non-concordant monazites are inheritance (e.g., Copeland et al., 1988), and reverse discordancy (e.g., Schärer, 1984). Reverse discordancy of a few Ma in the U-Pb system arises from excess ^{206}Pb due to incorporation of short-lived ^{230}Th during monazite crystallization (Schärer, 1984). Although reverse discordancy is a serious issue for precise U-Pb dating, particularly for young samples, it is not important for this work because counting statistics uncertainties are so large, and because Th decay is the greater contributor to total Pb. Inheritance (and Pb-loss) can be evaluated because X-ray mapping and spatially-precise analyses permit identification of zones that appear to be compositionally anomalous, both with respect to Th/U and Pb (Williams et al., 1999). Because we did not observe any chemically anomalous zones, we assume that inheritance was not a problem. The preservation of U-Th-Pb ages through melting and high-grade metamorphism, even at a scale of a few micrometers, supports nearly complete resistance to isotopic resetting (Copeland et al., 1988; DeWolf et al., 1993; Harrison et al., 1995; Watt, 1995; Zhu et al., 1997; Braun et al., 1998; Cocherie et al., 1998; Williams et al., 1999; Crowley and Ghent, 1999; Zhu and O'Nions, 1999). The consistency of ages determined on grains of different sizes supports an absence of either inheritance or significant Pb loss.

Ion microprobe Th-Pb analyses of large monazite grains were collected in situ with the Cameca ims 1270 housed at the Department of Earth and Space Sciences, University of California, Los Angeles. Monazite grains were first identified in thin section and mapped for Th, U, Y, and Si distributions by electron microprobe. Individual grains were then drilled out using a 0.25-in diamond drill corer, and mounted together with other samples and the UCLA 554 monazite standard in a 1-in epoxy round. Operating conditions are described by Harrison et al. (1995), and for this study involved a primary beam current of 6 to 12 nA, a spot size of ~10 μm, energy offsets for ^{232}Th$^+$ and ThO$_2$$^+$ of 15 and −8eV respectively, and a MRP of ~5000, which was sufficient to discriminate peak interferences. Total analysis time per spot was ~15 min. Common Pb corrections assumed Stacey-Kramers isotopic compositions (Stacey and Kramers, 1975), but alternative assumptions do not yield significantly different ages. Recently, it has been shown that there is a small REE-oxide interference with the ^{204}Pb peak, which can cause over-correction of common Pb, and hence too young an apparent age (Stern and Berman, 2001). Because there is so little common ^{208}Pb in our samples ($\ll$1%), potential changes to the correction imperceptibly affect ages. Reported age uncertainties reflect only counting statistics and the reproducibility of the ^{264}ThO$_2$$^+$/^{232}Th$^+$ vs. ^{208}Pb*$^+$/^{232}Th$^+$ calibration curve, as determined from multiple spots on the standard. These uncertainties are certainly minima for several reasons, including differences in preparation of standards vs. samples (e.g., single grains vs. polished sections), and averaging effects on the calibration curve confidence limits. For example, the overall age reproducibility on the standard was ~±1.2%, whereas the calculated age uncertainties for some spots on our samples are $<$ ±1% because their ^{264}ThO$_2$$^+$/^{232}Th$^+$ values fall towards the middle of the calibration curve. Although a reported error $<$ ±1% has statistical support, a more realistic error would be at least ±1 to 2% (Harrison et al., 1995).

Modes of monazite are useful for some calculations, and were determined via digital back-scattered electron images. Accurately determining monazite modes is surprisingly non-trivial. Although monazite crystals are readily identifiable, most grains are quite small (a few micrometers in diameter), and accurate measurements of areas require high-resolution images, e.g., at a 1-μm pixel resolution. However, a typical thin section has an area of ~1 × 10^9 μm^2, and would require prohibitively long times to characterize fully. We first assumed that grains were randomly distributed, and estimated modes by measuring only 10% of each section. However, we found that a few large grains can dominate the mode (≥90% of the total), and their distribution is non-random. Consequently, only the areas of the largest monazite grains were measured, which will underestimate modes slightly. A second complication is in assigning an appropriate threshold in digital images for estimating monazite areas because grain-boundaries often have anomalously high back-scattered electron yields. Changes in thresholding affected apparent monazite areas by ~10%. We chose to use the minimum threshold that still resolved monazite from other minerals, which maximizes the apparent modes of monazite. Uncertainties in monazite mode are at least ±10%.

3.1. Samples and Petrography

Approximately 100 samples were collected, principally from roadcuts, but also from outcrops along trails. Distributions of index minerals (garnet, staurolite and kyanite) conformed well with previous mapping (Hadley and Goldsmith, 1963). In the garnet zone, garnets are commonly idioblastic (Fig. 3A), whereas in the staurolite and kyanite zones they are rounded and embayed, and have biotite selvages (Figs. 3B and 3C). This texture results from the prograde staurolite-in reaction:

$$\mathit{Garnet} + \mathit{Muscovite} + \mathit{Chlorite} = \mathit{Biotite} + \mathit{Staurolite} + \mathit{Plagioclase} + \mathit{Quartz} + H_2O$$

Staurolite is idioblastic in the staurolite zone, but is rounded or embayed with biotite selvages in rocks that contain kyanite. This texture results from the prograde kyanite-in reaction:

$$\mathit{Staurolite} + \mathit{Muscovite} \pm \mathit{Chlorite} = \mathit{Garnet} + \mathit{Kyamite} + \mathit{Biotite} + H_2O$$

Kyanite is always idioblastic in samples unaffected by low-temperature retrogression. Note that a normal Barrovian progression of metamorphic reactions in metapelites involves low-grade garnet growth, intermediate-grade garnet consumption during staurolite production, and higher-grade resumption of garnet growth during staurolite consumption and kyanite production.

Monazite is virtually absent in substaurolite-grade rocks, and although an occasional tiny grain was found (diameter $<$ 5 μm), many occur in retrograde chlorite clots, and so may not be prograde. Apatite is abundant in all rocks, but no xenotime (YPO$_4$) was found. Mohr (1984) reports that allanite is present in some substaurolite-grade rocks but not in others. He does not identify specific allanite-bearing localities, but presumably these are from the stratigraphically higher Murphy Syncline to the southwest. Mapping of large portions of garnet-grade thin sections both with Ce, La, and P X-rays (4-μm resolution) and back-scattered electrons (≤1-μm resolution) failed to yield allanite or other REE silicates and oxides. This differs significantly from previous studies that have documented widespread allanite in substaurolite-grade regional and contact metamorphic rocks (Smith and Barreiro, 1990; Kingsbury et al., 1993; Ferry, 2000; Catlos et al., 2001; Wing et al., 2003). In contrast to lower grade rocks, monazite is ubiquitous in our staurolite and kyanite-bearing schists, which can contain hundreds of monazite grains per thin section in a variety of textures. For example, the field of view in Figure 3B is only ~2 mm^2, or $<$ 0.5% of the thin section, yet has nearly 35 optically distinguishable monazite grains. Grain diameters range from 1 to 2 μm to ~100 μm. Many of the smaller monazite grains are spatially associated with garnets, in biotite selvages (Figs. 3B and 3C), both within the matrix and as composite inclusions in staurolite. Insofar as these selvages are the result of the staurolite-in reaction, these monazite grains appear to be a byproduct. Other monazite grains are scattered throughout the rock. Large monazite crystals show no obvious association with other porphyroblasts, and occur both in the matrix and as inclusions in staurolite, plagioclase and kyanite (but not in garnet).

X-ray maps of large monazite grains (Fig. 4) and garnet (Fig. 5) provide additional information about the timing and mechanisms of monazite formation. Monazite grains ubiquitously exhibit quasi-continuous zoning from high-Th cores to low-Th rims, whereas Ce (and La) increase. Ca and Si also decrease towards the rim because they charge-balance Th^{4+} substitution for REE^{3+}. Y commonly shows a decrease from core to rim, but some grains additionally have higher-Y rims. Mohr (1984) first described this zoning but did not interpret it petrologically. Zoning is not completely smooth or radially symmetric, but the overall consistency of the core-rim chemical trends, particularly for Th, differs markedly from the zoning patterns documented for monazite grains in virtually all other metamorphic terranes. Most metamorphic monazite crystals exhibit a patchwork of chemical zones, with truncation of earlier-formed zoning patterns, replacement of crystal margins with chemically complex textures, and/or overall juxtaposition of distinct zones of radically different chemistry, likely because of dissolution and reprecipitation during multiple monazite growth events (e.g., Parrish, 1990; DeWolf et al., 1993; Zhu et al., 1997; Braun

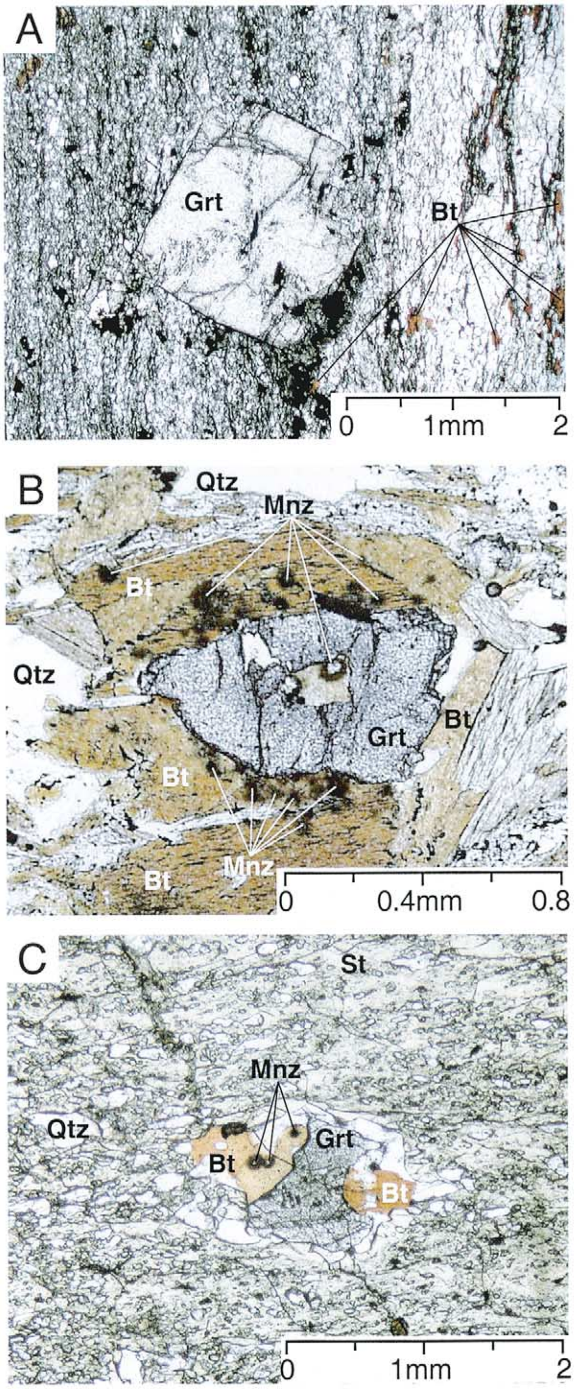

Fig. 3. Plane-polarized light photomicrographs of garnet and monazite textures. (A) Garnet from a garnet zone rock is idioblastic. Biotite grains are small, and not in contact with the garnet. Sample K00-45A. (B) In staurolite and kyanite zone rocks, garnet commonly has coronas of biotite, due to the garnet-consuming prograde reaction: Garnet + Chlorite + Muscovite = Biotite + Staurolite + Plagioclase + Quartz + H_2O. Monazite (spots) is abundant as inclusions in replacement biotite, which also happens to replace the center of this garnet. Monazite is common at staurolite- and kyanite-grade, yet extremely uncommon at garnet-grade. Sample K00-51C. (C) Garnet inclusion in staurolite (entire field of view) showing biotite selvage and monazite crystals (spots). Garnet commonly occurs as inclusions in staurolite and kyanite, which additionally contain inclusions of monazite. Apatite is the only phosphate that is included in relict garnets and garnet cores. Sample K00-17.

et al., 1998; Cocherie et al., 1998; Crowley and Ghent, 1999; Pyle and Spear, 1999, 2003; Williams et al., 1999; Zhu and O'Nions, 1999; Townsend et al., 2000; Pyle et al., 2001). In contrast, the chemical patterns from our samples are more consistent with fractional crystallization during a single monazite growth event. Because monazite partitions Th much more strongly than any other mineral in the rock, monazite growth quickly depletes matrix minerals in Th, and Th concentrations decrease. The increase in Ce simply reflects stoichiometric constraints. If Th, Ca, and Y decrease, the LREE's must increase. Even though LREE's are highly compatible in monazite, they partition less strongly compared to Th, and Th systematics thus dominate the overall chemical trends. These maps then imply that monazite growth was simple, perhaps via a single reaction, and did not obviously involve the dissolution-reprecipitation that has been inferred in other studies (e.g., Williams et al., 1999; Zhu and O'Nions, 1999; Townsend et al., 2000; Pyle et al., 2001; Pyle and Spear, 2003). Although there are small compositional irregularities to the zoning patterns, we ascribe these to relatively slow intergranular transport of a high valence elements like Y, REE's and/or Th, rather than to multiple monazite growth events. Steep vs. diffuse compositional gradients in these monazite crystals probably reflect slow vs. fast radial growth rates.

Major element maps of garnet show trends that are thoroughly typical of the amphibolite facies (Fig. 5; Spear et al., 1990). Mn decreases outward from the core, as expected for growth zoning (i.e., fractional crystallization and distillation of Mn as garnet grows with increasing temperature). Zoning in Ca and Mg is fairly smooth, and the increase in Mg towards the rim is consistent with garnet growth with increasing temperature. The increase in Mn and decrease in Mg right at the rim result from minor retrograde garnet dissolution, coupled with diffusional exchange with biotite (Spear and Florence, 1992). However, the regular zoning in major elements profoundly misrepresents the true reaction history that is implied by an annulus in Y, located approximately halfway between core and rim (Fig. 5D). The likeliest explanation for the Y annulus in this kyanite + staurolite–bearing rock is that it results from garnet dissolution (staurolite growth) followed by garnet regrowth as kyanite formed (Pyle and Spear, 1999). If the major element zoning in the garnet ever recorded this mineralogical event, then diffusion of divalent cations was sufficiently rapid to erase that record. Y and Mn both show increases at the rim of the garnet because of retrograde garnet dissolution at temperatures too low for Mn to homogenize. Of particular interest for monazite parageneses is that monazite grains occur not only in the matrix, but also as tiny (<5-μm diameter) inclusions in this garnet, immediately outside the Y annulus. Back-scattered electron images and P maps indicate that monazite is completely absent from garnet cores. Indeed, these are the only monazite inclusions in garnets that we have found that appear to have been trapped as the garnet grew. The only other monazite "inclusions" in garnet are associated with large clots of biotite and appear to replace the garnet core (e.g., Fig. 3B).

3.2. Metamorphic *P-T* Conditions

Preliminary *P-T* conditions were determined for a small subset of rocks from the garnet, staurolite, and kyanite zones (Tables 2 and 3). As discussed by Kohn and Spear (2000), accurate thermobarometry depends critically on collection of X-ray maps, and assessment of prograde and retrograde reactions on mineral compositions. In particular, retrograde net transfer reactions (ReNTRs) must be characterized because garnet dissolution can radically change matrix biotite compositions and calculated *P-T* calculations. Retrograde dissolution of garnets is evident in these rocks, both from major element (Mn) and trace element (Y) maps, which show increases in these elements at crystal boundaries. However, by using X-ray maps, one can correct for ReNTRs (Kohn and Spear, 2000). In samples analyzed so far, calculated corrections are so small (<10°C) that uncorrected compositions are essentially accurate. The retrieved *P-T* conditions (Table 3) are based on garnet compositions with the minimum Fe/(Fe + Mg), and yield pressures of 6 to 8 kbar, and temperatures of ~500°C (garnet zone) to ~600°C (staurolite and kyanite zones). Most important for this study, staurolite appears to have formed at a temperature of ~600°C, in excellent agreement with phase equilibria (e.g., Spear and Cheney, 1989), which predicts that staurolite should form between 575 and 600°C at 7 kbar.

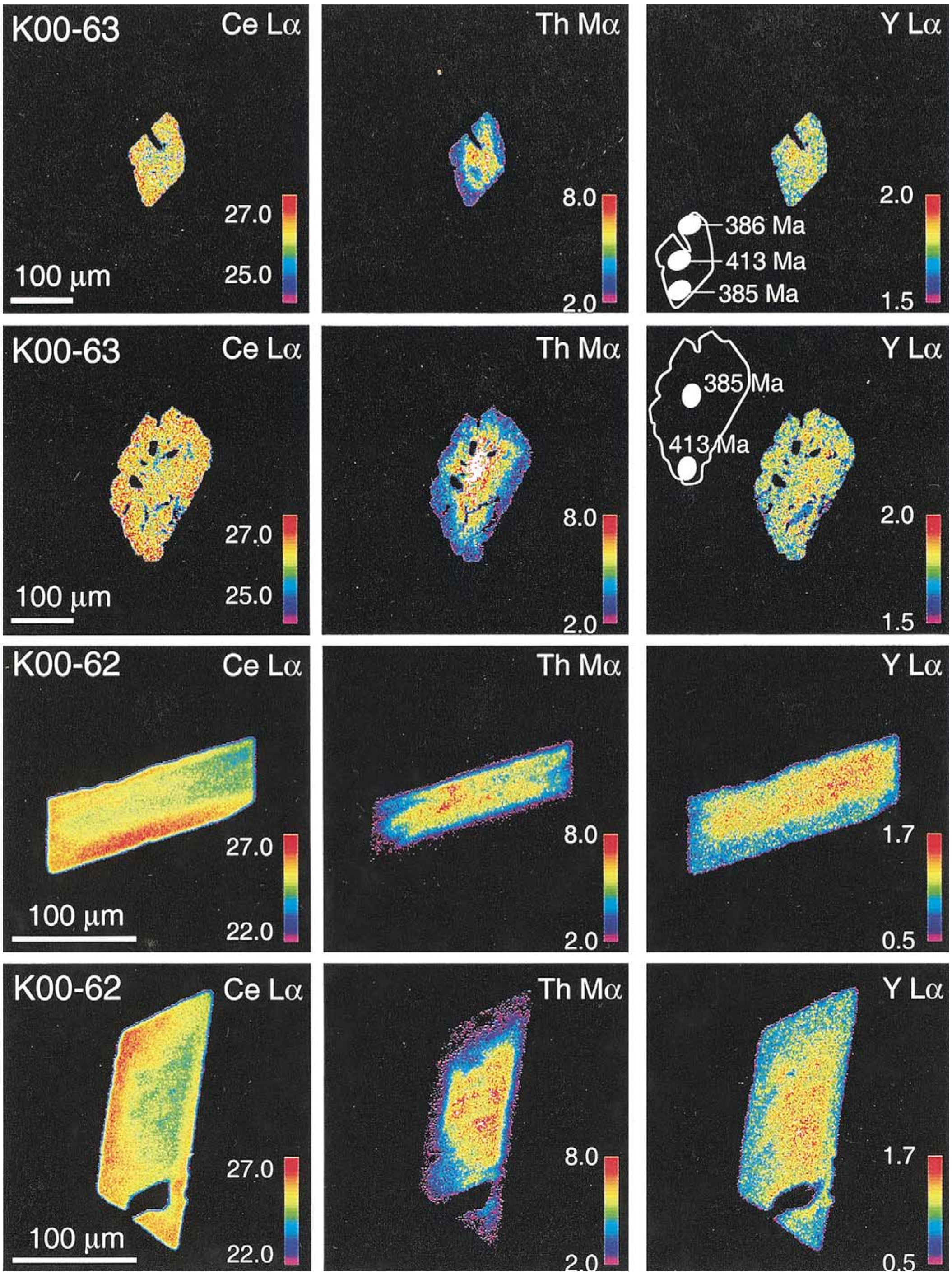

Fig. 4. X-ray maps of large monazite grains. Compositional scale bars are in wt.% Ce_2O_3, ThO_2, and Y_2O_3. Th and Y generally decrease towards rims, apparently due to fractional crystallization during growth. Ce increases towards rim, largely in compensation for fractionating monazite-compatible elements (Th and Y). Sketches in Y maps for K00-63 show locations and ages of ion microprobe spots for Th-Pb ages. Inclusions and cracks in the bottom grain are responsible for small compositionally anomalous regions.

3.3. Monazite Ages

Electron microprobe data (Table 4) are consistent with a single age of ~400 Ma (Fig. 6A). The spread in ages is entirely consistent with counting statistics uncertainties. These ages are all from relatively large (20–200-μm diameter) matrix grains or inclusions in kyanite and staurolite, and are not expected to reequilibrate (e.g., Lanzirotti and Hanson, 1997; Smith and Giletti, 1997; Cherniak et al., 2000). Ion microprobe ages on large, chemically zoned grains from the matrix of one sample (Table 5) yield a double-peaked distribution centered on ~400 Ma (Fig. 6B), with four ages each at ~385 and 415 Ma, and one age at ~400 Ma. However, assuming

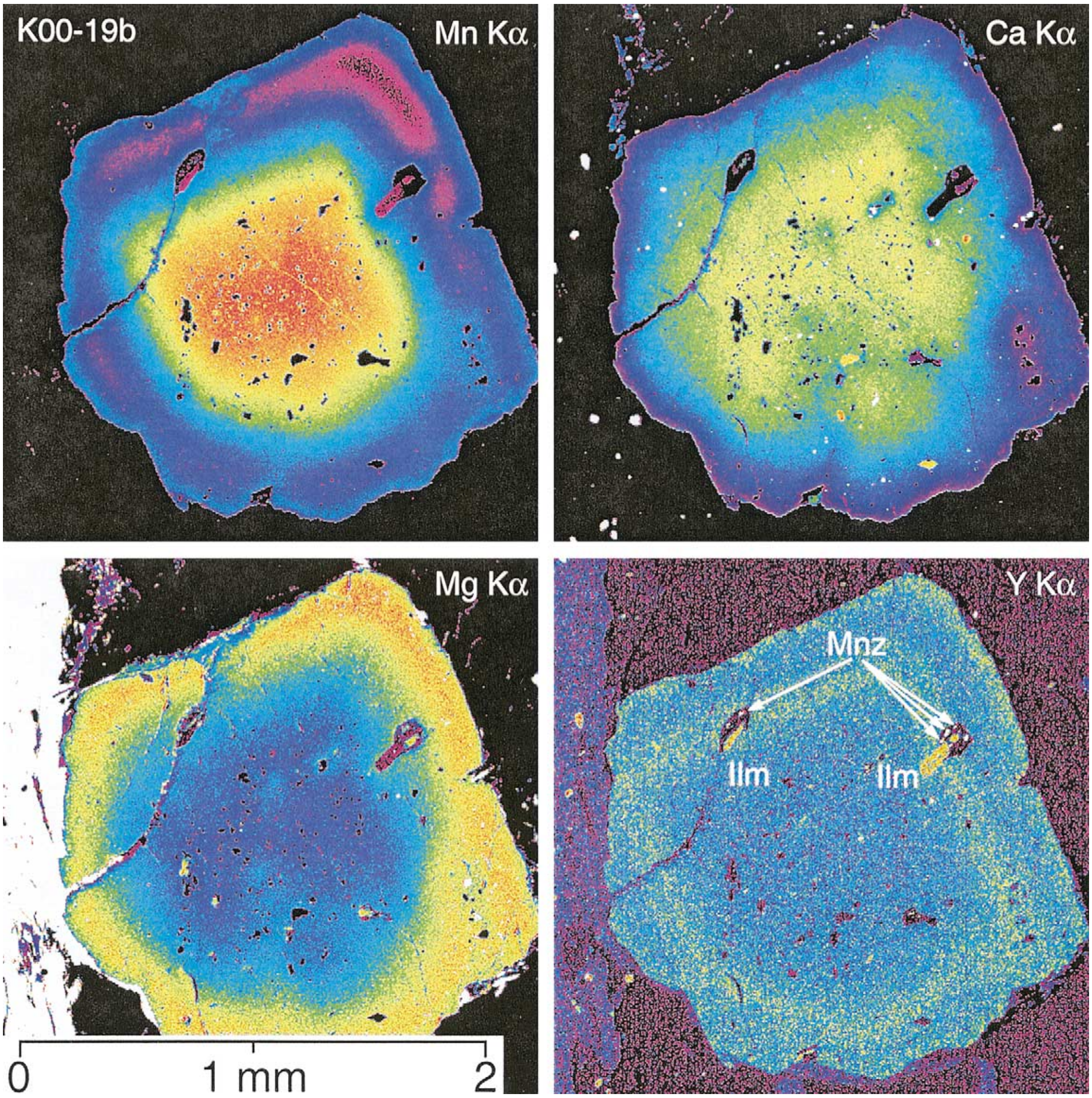

Fig. 5. X-ray maps of garnet. (A–C) Major elements show smooth zoning, with general rimward decreases in Mn and Ca, and an increase in Mg, typical of growth zoning. Near-rim increase in Mn and decrease in Mg is result of retrograde dissolution of garnet, with back-diffusion of Mn, and exchange of Fe and Mg with biotite. (D) A high-Y annulus results from garnet dissolution during staurolite growth, followed by regrowth of garnet with increasing temperature (Pyle and Spear, 1999). Occurrence of tiny (<5-μm diameter) monazite inclusions immediately outside the Y annulus is consistent with monazite formation during the staurolite-in reaction. Y-increase on rim of garnet also indicates garnet dissolution with back diffusion.

a minimal $\pm 1\sigma$ uncertainty of ± 5 Ma for each peak (i.e., equivalent to the $\pm 1.2\%$ age reproducibility on the standard, and lower than the $\pm 2\%$ calibration error described by Harrison et al., 1995), a χ^2 test indicates that these peaks are not statistically distinguishable at even 90% confidence. That is, the simplest explanation is that the Th-Pb age is ~400 Ma, and the double peak is an artifact of the small number of ages. This would also explain why there is no systematic relationship between core vs. rim ages (Fig. 4). The age uncertainty is relatively large, but the general consistency of ages observed among rocks and within crystals is expected if (1) growth of monazite in these rocks indeed occurred via a major isogradic reaction (staurolite-in) over a restricted temperature range (Spear and Cheney, 1989), and (2) monazite has high closure temperatures such that growth ages are preserved (Smith and Giletti, 1997; Cherniak et al., 2000).

4. INTERPRETATIONS

4.1. Monazite-Formation at the Staurolite-in Isograd

The increase in monazite abundance in staurolite- and higher-grade rocks, the spatial association of monazite with biotite selvages around garnet (both in the matrix and preserved as composite inclusions in staurolite), and the occurrence of monazite inclusions in garnet immediately outside a Y annulus all indicate that the staurolite-in isogradic reaction simultaneously produced monazite. Indeed, chemical zoning and textures in both staurolite zone and kyanite zone rocks indicate that the majority of monazite seems to have formed this way. These chemical and textual links further imply that reactions among

Table 2. Major element compositions of minerals from the Great Smoky Mountains, NC.

Sample	Muscovite, biotite, and chlorite							Garnet and plagioclase				
	50 Ms	50 Bt	30 Ms	30 Bt	38 Bt	42 Bt	47 Chl	50 Grt	30 Grt	38 Grt	42 Grt	47 Grt
Si	3.064	2.701	3.049	2.723	2.716	2.728	5.759	2.943	2.929	2.961	2.970	2.948
Al	2.767	1.697	2.811	1.712	1.702	1.645	5.159	2.039	2.058	2.033	2.031	2.023
Ti	0.047	0.094	0.028	0.085	0.087	0.112	0.012	0.001	0.000	0.004	0.001	0.004
Mg	0.080	1.254	0.077	1.153	1.187	0.916	5.542	0.435	0.414	0.389	0.146	0.249
Fe	0.055	1.153	0.061	1.205	1.203	1.458	3.117	2.372	2.351	2.361	1.998	1.468
Mn	0.000	0.000	0.002	0.005	0.004	0.010	0.061	0.092	0.055	0.003	0.545	1.070
Ca	0.000	0.000	0.000	0.000	0.000	0.002	0.000	0.155	0.180	0.216	0.325	0.275
Na	0.171	0.043	0.150	0.024	0.023	0.015	0.000					
K	0.814	0.869	0.829	0.886	0.872	0.920	0.005					
Fe/(Fe + Mg)		0.479		0.511	0.503	0.614	0.360	0.845	0.850	0.859	0.932	0.855
wt.% total	94.767	95.476	93.499	93.861	95.287	95.258	87.25	100.57	100.79	100.42	101.20	99.83
Plag An(%)								24	20	22	15	10

Sample numbers all have prefix of K00-. Compositions are normalized to an anhydrous oxygen basis of 12 (garnet), 11 (micas), and 28 (chlorite). Iron calculated assuming all Fe^{2+}.

common silicates can generally cause significant production or consumption of monazite. The aluminosilicate-in isograd has been proposed as an important reaction for stabilizing monazite (Ferry, 2000; Wing et al., 2003), based principally on changes in monazite modal abundances with increasing metamorphic grade. However, in those terranes, the aluminosilicate- and staurolite-isograds are almost coincident, and in our samples, where the isograds are distinct, there is no direct evidence from textures or zoning for production of monazite during the kyanite-in reaction. In Ferry's (2000) and Wing et al.'s (2003) rocks, allanite also is present at lower grades, and was a critical reactant. Apparently this LREE silicate destabilized during reactions among the other silicates relative to monazite. We have not found evidence for allanite, so we instead explore the possibility that reactions among the major silicates alone could form monazite, even in the absence of obvious LREE minerals.

One approach for evaluating this possibility is to use LREE and P compositions reported for major minerals in other rocks to calculate the amount of monazite that would be produced if recrystallization during reaction permitted these components to become available for monazite production. A similar calculation could be undertaken for Th and U, but because they are not commonly measured in silicates, and their average concentrations in our monazites are well over 1 order of magnitude lower than P and LREEs, results are less easily evaluated. Of the major silicates, only garnet, plagioclase, muscovite, biotite, and chlorite must be considered (Table 6) because quartz has such low concentrations of LREEs and P. In general, these calculations should reveal the maximum amount of monazite that could be produced, not only because preserved chemical zoning in garnet (and to a lesser extent, plagioclase) indicates that metamorphic minerals do not fully recrystallize during reactions, but also because the postreaction silicates will retain some (presumably lower) concentration of LREEs and P.

Although representative modes and P-contents of major minerals are readily assigned, LREE contents are more equivocal (Table 6). For reported compositions of major minerals plus apatite, the predicted whole-rock LREE content is at maximum ~30 ppm, whereas some rocks have higher LREE contents (up to ~100 ppm; e.g., Yang et al., 1999). This likely indicates that another LREE host (e.g., monazite) was present but unidentified in these rocks. If that host became stable because of reactions among major minerals during progressive metamorphism, and scavenged LREEs as it grew, then the measured LREE contents of the major minerals are now lower than they were before the reaction. For example, the micas can take as much as 100 ppm Ce + La (Dahl et al., 1993), and chlorite may possibly accept similar or larger amounts (Lanzirotti and Hanson, 1996). In the case of Lanzirotti and Hanson's (1996) study, the origin of such high LREE contents was ambiguous, as a

Table 3. Thermobarometric results[a] for rocks from the Great Smoky Mountains, NC.

Sample	K00-50	K00-30	K00-38	K00-42	K00-47
Grt-Bt (°C)[ab]	590	630	600	500	
Grt-Chl (°C)[ac]					460
GPMB/Q (bars)[d]	5800	7800	7600	6700[e]	7800[e]
Met. grade	Kyanite	Kyanite	Staurolite	Garnet	Garnet

[a] The Berman (1990) garnet solution model was used in all calculations. More recent solution models and thermobarometric calibrations do not significantly change calculations. Temperatures are reported at a pressure of 7 kbar and rounded to the nearest 10°C. If pressure were 5 kbar, apparent temperatures would be decreased by ~10°C. Pressures are reported at the apparent garnet - biotite temperature, and rounded to the nearest 100 bars. GPMB = Garnet - plagioclase - muscovite - biotite and Garnet - plagioclase - muscovite - quartz.

[b] Ferry and Spear (1978).

[c] Dickenson and Hewitt (1986) as corrected in Laird (1989).

[d] Hoisch (1990). Average of Fe and Mg endmember calibrations.

[e] The calculated pressure may be too high because the plagioclase composition is at or beyond the limits of applicability of the solution models.

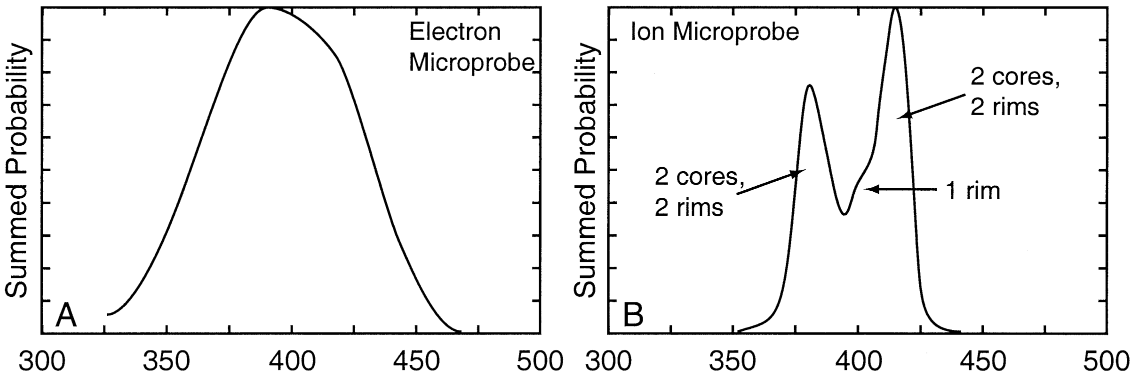

Fig. 6. Age probability diagrams, calculated by summing probability distributions of each age. Vertical scale is arbitrary. (A) Electron microprobe ages. Mean age is ~400 Ma. (B) Ion microprobe ages showing a double-peaked distribution centered on ~400 Ma. The lack of correspondence between core vs. rim ages and χ^2 test imply the peak separation could simply be an artifact of small number of analyses. Ages indicate that metamorphism occurred during the Acadian orogeny (~400 Ma), not during the Taconian (~450 Ma) as traditionally thought.

LREE-mineral was found intergrown with the chlorite, and could represent contamination, or alternatively exsolution during cooling. Regardless, these observations imply that from a LREE perspective, the tabulated "typical" compositions for the major silicates (Table 6) are minima, perhaps by as much as an order of magnitude.

In these predictive calculations, it is convenient to note that (1) a standard thin section has an area of $\sim 1 \times 10^9$ μm^2 (i.e., 10 cm^2), (2) most monazites contain ~50 wt.% LREE's and ~18.5 wt.% P, and (3) the density of monazite is ~1.9 times the density of the average crustal rock. Thus concentrations of 1 ppm P and 1 ppm LREE in a whole-rock, if converted to monazite, would correspond to monazite areas of ~2850 and 1050 μm^2 per thin section respectively. Monazite produces pleochroic haloes in biotite and has an extremely high backscattered electron yield. Consequently, even these tiny amounts of monazite could be readily observed, for example as a few hundred grains, several micrometers in diameter, especially if they were texturally associated with silicate reaction products. Conversely 10,000 μm^2 of monazite would contribute ~3.5 and ~9.5 ppm to whole-rock P- and LREE-contents. The P-contents of garnet and plagioclase easily accommodate major production of monazite, well in excess of 100,000 μm^2 per thin section, or over 1000 grains with a 10-μm diameter. Even considering incomplete recrystallization and the P-budgets of newly grown silicates, P is apparently non-limiting. The LREE contents of the major minerals are much less monazite-productive—only ~10,000 to 20,000 μm^2—but would still produce identifiable monazite. Adding apatite recrystallization to the LREE budget increases the calculated area of monazite by no more than ~10,000 μm^2. Increasing LREE contents of the micas and chlorite to 100 ppm would increase monazite areas by ~40,000 μm^2.

An alternative approach for evaluating the importance of reactions among major silicates for producing monazite is to (1) measure the mode of monazite in staurolite- and kyanite-bearing rocks, (2) assume monazite was produced solely by reactions among major silicates (i.e., excluding apatite and any LREE-minerals), and (3) calculate the concentrations of P and LREE that would be required to produce the observed amount of monazite. Conceptually, we simply "dissolve" the observed amount of monazite back into the major silicates and see

Table 4. Monazite electron microprobe ages.

Sample	Grain ID, size	Th (wt.%)	U (wt.%)	Pb (wt.%)	Y (wt.%)	Age (Ma)	$\pm 1\sigma$
K00-17a	Mtx-1, 20 μm	3.08	0.717	0.098	1.3	405	26
K00-17a	Mtx-1, 20 μm	3.04	0.793	0.103	1.5	411	26
K00-17a	Inclu-1, 20 μm	2.44	0.510	0.074	1.5	402	34
K00-19b	Mtx-5, 50 μm	2.92	0.669	0.090	1.8	394	28
K00-19b	Mtx-4, 50 μm	2.72	0.616	0.081	1.5	385	30
K00-19b	Mtx-4, 50 μm	2.51	0.643	0.076	1.6	368	31
K00-19b	Mtx-3, 100 μm	3.25	0.737	0.099	1.7	393	25
K00-19b	Mtx-3, 100 μm	3.09	0.678	0.100	1.6	422	27
K00-19b	Mtx-3, 100 μm	2.68	0.650	0.076	1.7	357	30
K00-63	Mtx-7, 100 μm	4.38	0.621	0.116	1.7	406	23
K00-63	Mtx-7, 100 μm	4.33	0.611	0.105	1.6	371	24
K00-63	Mtx-7, 100 μm	4.32	0.605	0.119	1.7	422	23
K00-63	Mtx-7, 100 μm	3.58	0.556	0.090	1.6	375	26
K00-63	Mtx-7, 100 μm	2.36	0.460	0.076	1.4	437	38

Errors are based on counting statistics uncertainty for Pb (typically ±65 ppm).

Table 5. Monazite ion microprobe Th-Pb ages for sample K00-63A.

Grain number	Age	$\pm 1\sigma$	^{208}Pb* (%)	U/Th	Core/rim
7	412.6	5.3	99.75	0.1022	Core
7	384.9	13.8	99.59	0.1254	Rim
7	386.2	4.9	99.43	0.1209	Rim
4	413.0	10.5	99.81	0.0729	Core
4	419.4	3.0	99.62	0.1513	Rim
6	384.8	8.1	99.77	0.0547	Core
6	413.2	3.3	99.40	0.1178	Rim
8	379.0	3.8	99.60	0.1082	Core
8	401.7	4.6	99.21	0.1264	Rim

Errors reflect only the measurement error on each Th-Pb age, and largely correspond to the calibration uncertainties. Percent radiogenic ^{208}Pb is: $\left[1 - \frac{(^{208}Pb/^{204}Pb)_{initial}}{(^{208}Pb/^{204}Pb)_{measured}}\right] \times 100\%$, where the initial Pb ratio was based on Stacey and Kramers (1975).

Table 6. Typical modes and trace element concentrations of metamorphic materials.

Mineral	Mode (%)	P (ppm)	P (%)	LREEs (ppm)	LREEs (%)
Quartz	35	0	0	0	0
Garnet	5	200	1–2	<1	0
Plagioclase	20	300	8–15	25–50	5–50
Staurolite	0	~0	0	0?	0?
Biotite	10	~0	0	10–20	1–10
Kyanite	0	~0	0	0?	0?
Muscovite	20	~0	0	10–20	2–20
Chlorite	10	~0	0	10?	1–5?
Sum majors:	100	70	9–17	9–17	9–85
Apatite	0.2–0.4	185,000	83–91	500–2500	1–50
Sum majors and apatite:	100	400–800	100	10–27	10–100
Whole rock (measured)		400–800		20–100	

Modes are based on the bulk composition of an average pelite at the staurolite-in isograd (Spear et al., 1990) and on whole-rock phosphorus contents of schists from the Great Smoky Mountains (~0.1–0.2 wt.% P_2O_5; Hadley and Goldsmith, 1963; Mohr, 1972). Phosphorus contents of minerals are based on electron microprobe measurements of minerals from the Great Smoky Mountains (unpublished data; see also summary of Spear and Pyle, 2002). Percent contribution to whole-rock P contents must sum to 100 because apatite mode was estimated from whole-rock P content. LREE contents of minerals are based on laser-ablation ICP-MS analyses of metamorphic rocks (Bea et al., 1994; Bea, 1996; Bea and Montero, 1999; Yang et al., 1999; Yang and Rivers, 2000, 2002). The percent contribution to whole-rock LREE contents assumes reported mineral compositions, typical modes, and reported schist compositions (Franz et al., 1996; Yang et al., 1999), and does not have to sum to 100 because whole-rock measurements could also have included LREE accessory minerals. Extreme LREE contents reported for pegmatite micas and metamorphic chlorite (100–500 ppm; Dahl et al., 1993; Lanzirotti and Hanson, 1996) have been omitted.

whether the implied concentrations of P and LREE's are compatible with measured concentrations in other rocks. The observed areas of monazite in staurolite- and kyanite-grade samples (Table 7), if produced from silicate reactions alone, would require only tens of parts per million P in the silicates, which is clearly available from plagioclase and garnet. However monazite modes also imply up to ~100 ppm LREEs in the sheet silicates and plagioclase, which is within the range of measured concentrations for these mineral groups (Dahl et al., 1993; Lanzirotti and Hanson, 1996), but ~5 to 10 times higher than has been commonly reported for metamorphic grains. This result implies either (1) a LREE accessory mineral (e.g., allanite) in fact was present before monazite growth, or (2) LREE contents of common metamorphic silicates can be higher than are typically reported, but decrease dramatically after a LREE accessory mineral is stabilized. We cannot rule out the possibility of premonazite LREE accessory minerals, but because inclusions, relict matrix grains, and mineralogies of rocks at lower grade have as yet yielded no evidence for them, we suggest that LREE contents of metamorphic silicates should be reevaluated.

4.2. Implications for Monazite Growth and Dating

From a mass balance perspective, major silicates contain sufficient P and LREEs that reactions among them could produce observable monazite, with tens of thousands of square micrometers per thin section. Obviously the presence of LREE reactants could strongly affect the amount of monazite produced and the metamorphic grade at which it appears. For example, metamorphic monazite in subgarnet and lower garnet zone rocks can form at the expense of Th-rich allanite (Catlos et al., 2001), and a large increase in monazite abundance can occur across the staurolite-in and aluminosilicate-in isograds because of allanite breakdown (Smith and Barreiro, 1990; Kingsbury et al., 1993; Ferry, 2000; Wing et al., 2003). In rocks where petrographic and chemical data link monazite growth with a major silicate reaction, such as staurolite-in (this study) or aluminosilicate-in (Ferry, 2000; Wing et al., 2003), the *P-T* conditions of monazite production can be uniquely assigned based on petrogenetic grids, thermobarometry, and/or *P-T* path analysis. In the case of the Smokies, the staurolite-in isograd occurs at ~600°C and 7 kbar, and U-Th-Pb geochronology indicates that this monazite formed at ~400 Ma.

Because many reactions may form monazite from major silicates and accessory minerals, including a variety of prograde reactions plus retrograde dissolution and reprecipitation, it is imperative that age investigations of metamorphic monazite first identify which reaction is responsible for the formation of each generation of monazite. This identification is best accomplished from composition maps of monazite grains and coexisting silicates, careful textural characterization of specific grains, and consideration of all reactions that have occurred, including those that involve not only LREE accessory minerals but also major silicates. Chemical characterization is particularly important because Pb diffusion in monazite is extremely slow (e.g., Smith and Giletti, 1997; Cherniak et al., 2000), leading to age heterogeneity among different domains (DeWolf

Table 7. Areas and modes of monazite for rocks from the Great Smoky Mountains, NC.

Sample	Grade	Area (μm^2)	Mode (%)	Contribution to whole-rock LREE and P (ppm)
K00-42	Garnet	<5000	<.0005	<5, <5
K00-47	Garnet	<5000	<.0005	<5, <5
K00-38b	Staurolite	50,000	.0070	~65, ~25
K00-50	Kyanite	50,000	.0055	~50, ~20
K00-63	Kyanite	75,000	.0070	~65, ~25

Monazite areas rounded to the nearest 5000 μm^2. Modes in percent are based on areas of monazite and total thin section, and can be converted to apparent contributions to whole-rock LREE and P concentrations by multiplying by ~9500 and ~3500 respectively.

et al., 1993; Zhu et al., 1997; Braun et al., 1998; Cocherie et al., 1998; Crowley and Ghent, 1999; Williams et al., 1999; Zhu and O'Nions, 1999). The chemical behavior of monazite is analogous to zircon, where inheritance and overgrowths are expected and should be characterized before any age determinations. If a petrogenetic model cannot be developed for monazite growth in a particular rock, then ages will have minimal significance. In xenotime-absent rocks, most of the silicate reactions that have been proposed to form monazite simultaneously (e.g., Smith and Barreiro, 1990; Kingsbury et al., 1993; Pyle and Spear, 2003; this study) in fact consume garnet, which has high concentrations of P. Possibly P-fluxes during garnet dissolution are key for producing monazite.

4.3. Tectonic Implications

A detailed discussion of the *P-T* evolution and tectonic implications requires more complete petrologic and geochronologic characterization. However in general the ages imply that the main metamorphic event of the southern Laurentian margin was Acadian in age, not Taconian, supporting stratigraphic arguments (Unrug and Unrug, 1990; Unrug et al., 1991, 2000) that deformation and metamorphism were post-Silurian. In contrast, the EBR arc terranes immediately outboard of the WBR and Laurentian margin clearly underwent Ordovician ("Taconian") metamorphism (Goldberg and Dallmeyer, 1997; Trupe, 1997; Miller et al., 2000). The younger age for metamorphism on the margin of Laurentia implies that initial Taconian metamorphism of the EBR occurred before full accretion to Laurentia. This pattern in the southern Appalachians differs from the tectonic evolution of the northern Appalachians, where arc-terranes accreted with Laurentia in the Taconian (e.g., Robinson et al., 1998), and there are clear age-distinctive, high-grade metamorphic belts of inboard Taconian vs. outboard Acadian metamorphic rocks (Laird et al., 1984; Sutter et al., 1985; Robinson et al., 1998). Whereas the tectonic evolution of the southern Appalachians is in many ways analogous to other sections of the orogen, it also differs in some critical ways, most importantly in the timing and sequence of terrane accretion.

5. CONCLUSIONS

Abundances and textures of monazite, and chemical zoning patterns in both monazite and garnet from the Great Smoky Mountains indicate that major monazite production occurred during the staurolite-in reaction. Although we cannot rule out the possibility that a precursor LREE mineral was present, garnet, plagioclase, and sheet silicates host sufficient P and LREEs that reaction among them could stabilize petrographically observable monazite. This then implies that other reactions among common metamorphic silicates could control the growth or dissolution of monazite at various grades (Ferry, 2000; Pyle and Spear, 2003; Wing et al., 2003). Because Pb diffusion in monazite is so slow (Smith and Giletti, 1997; Cherniak et al., 2000), such episodic growth or dissolution is likely to be recorded by domains of different chemistries and ages, perhaps explaining why so many metamorphic monazite crystals exhibit such complex internal zonation. Ultimately, ascribing age significance to monazite analyses will require first assessing likely prograde reactions that can form monazite, including common silicate reactions. Conversely, if the likely metamorphic reactions responsible for monazite growth are not characterized, then ages of whole monazite grains, or even small spots, are seriously devalued. Documentation of mineralogical textures and internal chemical and age zonation is of paramount importance. For example, the new age determinations for the Smokies coupled with definitive information on the *P-T* conditions of monazite growth demonstrate that metamorphism on the southeastern margin of Laurentia, was Devonian (~400 Ma), rather than Ordovician. This then implies that orogenic evolution of the southern Appalachians proceeded differently than in the northern Appalachians.

Acknowledgments—Funded by NSF grant EAR 0073803, and a grant from USC. Reviews from J. Ferry, G. Franz, and C. Daniel significantly improved the MS, although their views do not necessarily coincide with those presented here. We thank M. Williams for alerting us to the possibility of C-coat damage during electron microprobe analysis, J. Pyle and F. Spear for sending us the $PbSiO_3$ standard, and K. Langdon at Great Smoky Mountains National Park for permitting sample collection.

Associate editor: F. J. Ryerson

REFERENCES

Bea F. (1996) Residence of REE, Y, Th and U in granites and crustal protoliths; implications for the chemistry of crustal melts. *J. Petrol.* **37**, 521–552.

Bea F. and Montero P. (1999) Behavior of accessory phases and redistribution of Zr, REE, Y, Th, and U during metamorphism and partial melting of metapelites in the lower crust; an example from the Kinzigite Formation of Ivrea-Verbano, NW Italy. *Geochim. Cosmochim. Acta* **63**, 1133–1153.

Bea F., Pereira M. D., and Stroh A. (1994) Mineral/leucosome trace-element partitioning in a peraluminous migmatite (a laser ablation-ICP-MS study). *Chem. Geol.* **117**, 291–312.

Berman R. G. (1990) Mixing properties of Ca-Mg-Fe-Mn garnets. *Am. Mineral.* **75**, 328–344.

Bingen B., Demaiffe D., and Hertogen J. (1996) Redistribution of rare earth elements, thorium, and uranium over accessory minerals in the course of amphibolite to granulite facies metamorphism; the role of apatite and monazite in orthogneisses from southwestern Norway. *Geochim. Cosmochim. Acta* **60**, 1341–1354.

Braun I., Montel J.-M., and Nicollet C. (1998) Electron microprobe dating of monazites from high-grade gneisses and pegmatites of the Kerala khondalite belt, southern India. *Chem. Geol.* **146**, 65–85.

Brosky R. and Odom L. (2002) U-Pb staurolite age of metamorphism in the western Blue Ridge, southern Appalachians. *Geol. Soc. Am. Abstr. Prog.* **34**, 342.

Catlos E., Harrison T. M., Kohn M. J., Grove M., Lovera O. M., Ryerson F. J., and Upreti B. N. (2001) Geochronologic and thermobarometric constraints on the evolution of the Main Central Thrust, central Nepal Himalaya. *J. Geophys. Res.* **106**, 16177–16203.

Cherniak D. J., Watson E. B., Harrison T. M., and Grove M. (2000) Pb diffusion in monazite: A progress report on a combined RBS/SIMS study. *Eos: Trans. Am. Geophys. Union* **81**, S25.

Cocherie A., Legendre O., Peucat J. J., and Kouamelan A. N. (1998) Geochronology of polygenetic monazites constrained by in situ electron microprobe Th-U-total lead determination; implications for lead behaviour in monazite. *Geochim. Cosmochim. Acta* **62**, 2475–2497.

Connelly J. B. and Woodward N. B. (1992) Taconian foreland-style thrust system in the Great Smoky Mountains, Tennessee. *Geology* **20**, 177–180.

Connelly J. B. and Dallmeyer R. D. (1993) Polymetamorphic evolution of the western Blue Ridge; evidence from $^{40}Ar/^{39}Ar$ whole-rock slate/phyllite and muscovite ages. *Am. J. Sci.* **293**, 322–359.

Cook F. A., Albaugh D. S., Brown L. D., Kaufman S., Oliver J. E., and Hatcher R. D. Jr. (1979) Thin-skinned tectonics in the crystalline southern Appalachians; COCORP seismic-reflection profiling of the Blue Ridge and Piedmont. *Geology* **7**, 563–567.

Cook F. A., Brown L. D., Kaufman S., Oliver J. E., and Petersen T. A. (1981) COCORP seismic profiling of the Appalachian Orogen beneath the coastal plain of Georgia. *Geol. Soc. Am. Bull.* **92**, I738–I748.

Copeland P., Parrish R. R., and Harrison T. M. (1988) Identification of inherited radiogenic Pb in monazite and its implications for U-Pb systematics. *Nature* **333**, 760–763.

Crowley J. L. and Ghent E. D. (1999) An electron microprobe study of the U-Th-Pb systematics of metamorphosed monazite; the role of Pb diffusion versus overgrowth and recrystallization. *Chem. Geol.* **157**, 285–302.

Cumbest R. J., Johnson E. L., and Onstott T. C. (1994) Argon composition of metamorphic fluids; implications for ^{40}Ar/^{39}Ar geochronology. *Geol. Soc. Am. Bull.* **106**, 942–951.

Dahl P. S., Wehn D. C., and Feldmann S. G. (1993) The systematics of trace-element partitioning between coexisting muscovite and biotite in metamorphic rocks from the Black Hills, South Dakota, USA. *Geochim. Cosmochim. Acta* **57**, 2487–2505.

Dallmeyer R. D. (1975) ^{40}Ar/^{39}Ar age spectra of biotite from Grenville basement gneisses in Northwest Georgia. *Geol. Soc. Am. Bull.* **86**, 1740–1744.

Dallmeyer R. D. (1988) Polymetamorphic evolution of the western Blue Ridge allochthon: Evidence from ^{40}Ar/^{39}Ar mineral ages. In *Geology of the Murphy Belt and Related Rocks—Georgia and North Carolina, Vol. 8* (eds. W. J. Fritz and F. L. LaTour), pp. 95–101. Georgia Geological Society.

DeWolf C. P., Belshaw N. S., and O'Nions R. K. (1993) A metamorphic history from micron-scale ^{207}Pb/^{206}Pb chronometry of Archean monazite. *Earth Planet. Sci. Lett.* **120**, 207–220.

Dickenson M. P. and Hewitt D. (1986) A garnet-chlorite geothermometer. *Geol. Soc. Am. Abstr. Prog.* **18**, 584.

Drake M. J. and Weill D. F. (1972) New rare earth element standards for electron microprobe analysis. *Chem. Geol.* **10**, 179–181.

Ferry J. M. (2000) Patterns of mineral occurrence in metamorphic rocks. *Am. Mineral.* **85**, 1573–1588.

Ferry J. M. and Spear F. S. (1978) Experimental calibration of the partitioning of Fe and Mg between biotite and garnet. *Contrib. Mineral. Petrol.* **66**, 113–117.

Franz G., Andrehs G., and Rhede D. (1996) Crystal chemistry of monazite and xenotime from Saxothuringian-Moldanubian metapelites, NE Bavaria, Germany. *Eur. J. Mineral.* **8**, 1097–1118.

Goldberg S. A. and Dallmeyer R. D. (1997) Chronology of Paleozoic metamorphism and deformation in the Blue Ridge thrust complex, North Carolina and Tennessee. *Am. J. Sci.* **297**, 488–526.

Hadley J. B. and Goldsmith R. (1963) *Geology of the Eastern Great Smoky Mountains North Carolina and Tennessee*. USGS Professional Paper.

Hames W. E., Tracy R. J., Ratcliff N. M., and Sutter J. F. (1991) Petrologic, structural and geochronologic characteristics of the Acadian metamorphic overprint on the Taconian zone in part of southwestern New England. *Am. J. Sci.* **291**, 887–913.

Harrison T. M. (1981) Diffusion of ^{40}Ar in hornblende. *Contrib. Mineral. Petrol.* **78**, 324–331.

Harrison T. M., McKeegan K. D., and LeFort P. (1995) Detection of inherited monazite in the Manaslu leucogranite by ^{208}Pb/^{232}Th ion microprobe dating: Crystallization age and tectonic significance. *Earth Planet. Sci. Lett.* **133**, 271–282.

Hatcher R. D. (1987) Tectonics of the southern and central Appalachian internides. *Ann. Rev. Earth Planet. Sci.* **15**, 337–362.

Heaman L. and Parrish R. (1991) U-Pb geochronology of accessory minerals. In *Applications of Radiogenic Isotope Systems to Problems in Geology Short Course Handbook, Vol. 19* (eds. L. Heaman and J. N. Ludden), pp. 59–102. Mineralogical Association of Canada.

Hibbard J. (2000) Docking Carolina: Mid-Paleozoic accretion in the southern Appalachians. *Geology* **28**, 127–130.

Hoisch T. D. (1990) Empirical calibration of six geobarometers for the mineral assemblage quartz+muscovite+biotite+plagioclase+garnet. *Contrib. Mineral. Petrol.* **104**, 225–234.

Kingsbury J. A., Miller C. F., Wooden J. L., and Harrison T. M. (1993) Monazite paragenesis and U-Pb systematics in rocks of the eastern Mojave Desert, California, U.S.A; implications for thermochronometry. *Chem. Geol.* **110**, 147–167.

Kohn M. J. (2001) Timing of arc accretion in the southern Appalachians: Perspectives from the Laurentian margin. *Geol. Soc. Am. Abstr. Prog.* **33,** A-262.

Kohn M. J. and Spear F. S. (2000) Retrograde net transfer reaction insurance for pressure-temperature estimates. *Geology* **28**, 1127–1130.

Laird J. (1989) Chlorites: Metamorphic petrology. *Rev. Mineral.* **19**, 405–453.

Laird J., Lanphere M. A., and Albee A. L. (1984) Distribution of Ordovician and Devonian metamorphism in mafic and pelitic schists from northern Vermont. *Am. J. Sci.* **284**, 376–413.

Lanzirotti A. and Hanson G. N. (1996) Geochronology and geochemistry of multiple generations of monazite from the Wepawaug Schist, Connecticut, USA: Implications for monazite stability in metamorphic rocks. *Contrib. Mineral. Petrol.* **125**, 332–340.

Lanzirotti A. and Hanson G. N. (1997) An assessment of the utility of staurolite in U-Pb dating of metamorphism. *Contrib. Mineral. Petrol.* **129**, 352–365.

Miller B. V., Stewart K. G., Miller C. F., and Thomas C. W. (2000) U-Pb ages from the Bakersville, North Carolina eclogite: Taconian eclogite metamorphism followed by Acadian and Alleghanian cooling. *Geol. Soc. Am. Abstr. Prog.* **32,** A-62.

Mohr D. W. (1972) *Stratigraphy, Structure, and Metamorphism of the Eastern Part of the Fontana Lake Reservoir, Great Smoky Mountains, North Carolina*. Ph.D. dissertation, University of Michigan.

Mohr D. W. (1984) Zoned porphyroblasts of metamorphic monazite in the Anakeesta Formation, Great Smoky Mountain, North Carolina. *Am. Mineral.* **69**, 93–103.

Mohr D. W. and Newton R. C. (1983) Kyanite-staurolite metamorphism in sulfidic schists of the Anakeesta Formation, Great Smoky Mountains, North Carolina. *Am. J. Sci.* **283**, 97–134.

Montel J.-M., Foret S., Veschambre M., Nicollet C., and Provost A. (1996) Electron microprobe dating of monazite. *Chem. Geol.* **131**, 37–53.

Neuman R. B. (1955) Middle Ordovician rocks of the Tellico-Sevier belt, eastern Tennessee. *U.S. Geol. Surv. Prof. Paper* **274-F**, 141–177.

Parrish R. R. (1990) U-Pb dating of monazite and its application to geological problems. *Can. J. Earth Sci.* **27**, 1431–1450.

Pyle J. M. and Spear F. S. (1999) Yttrium zoning in garnet: coupling of major and accessory phases during metamorphic reactions. *Geol. Mat. Res.* **1**, 1–49.

Pyle J. M. and Spear F. S. (2003) Four generations of accessory-phase growth in low-pressure migmatites from SW New Hampshire. *Am. Mineral.* **88**, 338–351.

Pyle J. M., Spear F. S., Rudnick R. L., and McDonough W. F. (2001) Monazite-xenotime-garnet equilibrium in metapelites and a new monazite-garnet thermometer. *J. Petrol.* **42**, 2083–2107.

Pyle J. M., Spear F. S., and Wark D. A. (2002) Protocols and pitfalls in electron microprobe analysis of phosphate minerals. *Rev. Mineral.* **48**, 337–362.

Rasmussen B., Fletcher I. R., and McNaughton N. J. (2001) Dating low-grade metamorphic events by SHRIMP U-Pb analysis of monazite in shales. *Geology* **29**, 963–966.

Robinson P., Tucker R. D., Bradley D., Berry H. N., and Osberg P. H. (1998) Paleozoic orogens in New England, USA. *GFF.* **120**, 119–148.

Rodgers J. (1953) *Geological Map of East Tennessee With Explanatory Text*. Tennessee Department of Conservation.

Rodgers J. (1971) The Taconic orogeny. *Geol. Soc. Am. Bull.* **82**, 1141–1178.

Schärer U. (1984) The effect of initial ^{230}Th disequilibrium on young U-Pb ages; the Makalu case, Himalaya. *Earth Planet. Sci. Lett.* **67**, 191–204.

Scherrer N. C., Engi M., Gnos E., Jakob V., and Liechti A. (2000) Monazite analysis; from sample preparation to microprobe age dating and REE quantification. *Schweiz Mineral. Petrograph. Mitteil.* **80**, 93–105.

Smith H. A. and Barreiro B. (1990) Monazite U-Pb dating of staurolite grade metamorphism in pelitic schists. *Contrib. Mineral. Petrol.* **105**, 602–615.

Smith H. A. and Giletti B. J. (1997) Lead diffusion in monazite. *Geochim. Cosmochim. Acta* **61**, 1047–1055.

Spear F. S. and Cheney J. T. (1989) A petrogenetic grid for pelitic schists in the system SiO_2-Al_2O_3-FeO-MgO-K_2O-H_2O. *Contrib. Mineral. Petrol.* **101**, 149–164.

Spear F. S. and Florence F. P. (1992) Thermobarometry in granulites: Pitfalls and new approaches. *J. Precam. Res.* **55**, 209–241.

Spear F. S. and Pyle J. M. (2002) Phosphates in metamorphic rocks. *Rev. Mineral.* **48**, 293–335.

Spear F. S., Kohn M. J., Florence F., and Menard T. (1990) A model for garnet and plagioclase growth in pelitic schists: Implications for thermobarometry and *P-T* path determinations. *J. Metamorph. Geol.* **8**, 683–696.

Stacey J. S. and Kramers J. D. (1975) Approximation of terrestrial lead isotope evolution by a two-stage model. *Earth Planet. Sci. Lett.* **26**, 207–221.

Stern R. A. and Berman R. G. (2001) Monazite U-Pb and Th-Pb geochronology by ion microprobe, with an application to in situ dating of an Archean metasedimentary rock. *Chem. Geol.* **172**, 113–130.

Sutter J. F., Ratcliff N. M., and Mukasa S. B. (1985) $^{40}Ar/^{39}Ar$ and K-Ar data bearing on the metamorphic and tectonic history of western New England. *Geol. Soc. Am. Bull.* **96**, 123–136.

Suzuki K. and Adachi M. (1998) Denudation history of the high T/P Ryoke metamorphic belt, Southwest Japan; constraints from CHIME monazite ages of gneisses and granitoids. *J. Metamorph. Geol.* **16**, 23–37.

Townsend K. J., Miller C. F., D'Andrea J. L., Ayers J. C., Harrison T. M., and Coath C. D. (2000) Low temperature replacement of monazite in the Ireteba Granite, southern Nevada; geochronological implications. *Chem. Geol.* **172**, 95–112.

Trupe C. H. III (1997) *Deformation and Metamorphism in Part of the Blue Ridge Thrust Complex, Northwestern North Carolina*. Ph.D. dissertation, University of North Carolina, Chapel Hill.

Unrug R. and Unrug S. (1990) Paleontological evidence of Paleozoic age for the Walden Creek Group, Ocoee Supergroup, Tennessee. *Geology* **18**, 1041–1045.

Unrug R., Unrug S., and Palmes S. L. (1991) Carbonate rocks of the Walden Creek Group in the Little Tennessee River Valley: Modes of occurrence, age and significance for the basin evolution of the Ocoee Supergroup. In *Studies of the Precambrian and Paleozoic Stratigraphy in the Western Blue Ridge* (ed. S. A. Kish), pp. 27–36. Carolina Geological Society.

Unrug R., Ausich W. I., Bednarczyk J., Cuffey R. J., Mamet B. L., Palmes S. L., and Unrug S. (2000) Paleozoic age of the Walden Creek Group, Ocoee Supergroup, in the western Blue Ridge, Southern Appalachians; implications for evolution of the Appalachian margin of Laurentia. *Geol. Soc. Am. Bull.* **112**, 982–996.

Watt G. R. (1995) High-thorium monazite-(Ce) formed during disequilibrium melting of metapelites under granulite-facies conditions. *Miner. Mag.* **59**, 735–743.

Williams M. L., Jercinovic M. J., and Terry M. P. (1999) Age mapping and dating of monazite on the electron microprobe; deconvoluting multistage tectonic histories. *Geology* **27**, 1023–1026.

Wing B. N., Ferry J. M., and Harrison T. M. (in press) Prograde destruction and formation of monazite and allanite during contact and regional metamorphism of pelites: Petrology and geochronology. *Contrib. Mineral. Petrol* **145,** 228–250.

Woodward N. B., Connelly J. B., Walters R. R., and Lewis J. C. (1991) Tectonic evolution of the Great Smoky Mountains. In *Studies of Precambrian and Paleozoic Stratigraphy in the Western Blue Ridge* (ed. S. A. Kish), pp. 45–56. Carolina Geological Society.

Yang P. and Rivers T. (2000) Trace element partitioning between coexisting biotite and muscovite from metamorphic rocks, western Labrador; structural, compositional and thermal controls. *Geochim. Cosmochim. Acta* **64**, 1451–1472.

Yang P. and Rivers T. (2002) The origin of Mn and Y annuli in garnet and the thermal dependence of P in garnet and Y in apatite in calc-pelite and pelite, Gagnon terrane, western Labrador. *Geol. Mat. Res.* **4,** http://gmr.minsocam.org/contents.html.

Yang P., Rivers T., and Jackson S. J. (1999) Crystal-chemical and thermal controls on trace-element partitioning between coexisting garnet and biotite in metamorphic rocks from western Labrador. *Can. Mineral.* **37**, 443–486.

Zhu X. K. and O'Nions R. K. (1999) Zonation of monazite in metamorphic rocks and its implications for high temperature thermochronology; a case study from the Lewisian terrain. *Earth Planet. Sci. Lett.* **171**, 209–220.

Zhu X. K., O'Nions R. K., Belshaw N. S., and Gibb A. J. (1997) Significance of in situ SIMS chronometry of zoned monazite from the Lewisian granulites, Northwest Scotland. *Chem. Geol.* **135**, 35–53.

Appendix

A.1. Electron Microprobe Analytical Concerns

Small errors in placement of backgrounds, peak interferences, and spectrometer and sample idiosyncracies can propagate to relatively large errors in apparent trace element concentration and age. Some specific problems include:

1. Peak overlap for U. The tail of the Th M_γ peak overlaps U M_β. Analysis of pure ThO_2 indicates a correction factor of -55 ± 3 ppm U/wt.% Th for our electron microprobe, similar to a calculated value of -52 ppm U/wt.% Th (Scherrer et al., 2000). Correction terms may vary depending on the quality of the PET crystal used.
2. Peak interferences for Pb. Two Pb peaks may be analyzed (M_α or M_β), and both have major peak interferences. The Pb M_α peak has interferences with both YL_α (Montel et al., 1996) and ThM_z (Scherrer et al., 2000) which, if uncorrected, can cause inaccuracies of up to ~100 ppm in Pb. However, accurate correction factors can be estimated based on analysis of YAG (-67 ± 2 ppm Pb/wt.% Y_2O_3) and ThO_2 (-3 ppm Pb/wt.% ThO_2), so that Pb correction uncertainties are typically $\leq \pm 5$ppm. The Pb M_β peak has a major interference with the tail of a second-order Ce $L\alpha$ peak. The Ce interference can be screened out using pulse-height analysis, but even with this screening, extraneous signal arises on spectrometers that use P-10 counters, which Pyle et al. (2002) suggest is due to an Ar escape peak. Such extraneous counts are absent for the Pb M_β peak on Xe counters. Because the USC electron microprobe has P-10 counters, we used the Pb M_α peak.
3. Standardization errors for Pb. The background on Pb standards between the Pb M_α and M_β peaks is always above baseline for our PET crystals (as determined on Pb-poor materials). The contribution of the faulty background to age uncertainty is only ~0.3% and was ignored in this study. Single-sided background measurements during standardization could overcome this problem, or all ages could be systematically decreased by 0.3%.
4. Spot size and carbon coat. Different spot sizes do not affect Th, U, and Pb measurements on our standards, but the absorbed current on monazite grains in a typical polished thin section can change during analysis if the beam size is too small. If absorbed current varies, then X-ray intensities likely also vary, compromising the accuracy of an analysis. Current drift is associated not only with visible damage to the carbon coat, but also with age scatter beyond counting statistics errors for grains that we believe should be chronologically homogeneous. This effect is pronounced when the beam is focused to 5 μm or less, but completely absent for a spot size of 20 μm. We do not fully understand this phenomenon. Some of our monazite grains are at least as large as our standards, so grain size or proximity to grain boundaries is not an obvious source. Possibly the result is idiosyncratic to the carbon coat, so that coats sputtered on different days have different susceptibilities to electron beam damage, and our standards fortuitously have a "good" coat. Regardless, we ensured our spot sizes were large enough so that the current did not drift during analysis, which we believe also yields the most precise and accurate results.

The corrections introduce additional uncertainties, but assuming they are randomly distributed, a typical total error would be $\sim\pm 65$ ppm, as calculated from the square root of the sum of the squares of ± 65 ppm (counting statistics) and ± 5 ppm (correction errors for peak interferences on Pb).